

Evidence for Large-Scale Cold Gas Outflows Associated with Nuclear Winds in Reionization-Era Quasars

Yongda Zhu^{1,†}, Marcia J. Rieke¹, Luis C. Ho^{2,3}, Yang Sun¹, George H. Rieke¹, Feng Yuan⁴, Tom J. L. C. Bakx⁵, George D. Becker⁶, Jinyi Yang⁷, Eduardo Bañados⁸, Manuela Bischetti⁹, Christopher Cain¹⁰, Xiaohui Fan¹, Yoshinobu Fudamoto^{11,1}, Seyedazim Hashemi⁶, Ryota Ikeda^{12,13}, Zhiyuan Ji¹, Xiangyu Jin¹, Weizhe Liu¹, Yichen Liu¹, Jianwei Lyu¹, Hai-Xia Ma¹⁴, Tsutomu T. Takeuchi^{14,15}, Hideki Umehata^{16,17}, Feige Wang⁷, Wei Leong Tee¹

¹Steward Observatory, University of Arizona, 933 North Cherry Avenue, Tucson, AZ 85721, USA; ²Kavli Institute for Astronomy and Astrophysics, Peking University, Beijing 100871, China; ³Department of Astronomy, School of Physics, Peking University, Beijing 100871, China; ⁴Center for Astronomy and Astrophysics and Department of Physics, Fudan University, Shanghai 200438, China; ⁵Department of Space, Earth, & Environment, Chalmers University of Technology, Chalmersplatsen 4, 412 96 Gothenburg, Sweden; ⁶Department of Physics & Astronomy, University of California, Riverside, CA 92521, USA; ⁷Department of Astronomy, University of Michigan, 1085 S. University, Ann Arbor, MI 48109, USA; ⁸Max-Planck-Institut für Astronomie, Königstuhl 17, D-69117 Heidelberg, Germany; ⁹Dipartimento di Fisica, Sezione di Astronomia, Università di Trieste, via Tiepolo 11, 34143 Trieste, Italy; ¹⁰School of Earth and Space Exploration, Arizona State University, Tempe, AZ 85287-6004, USA; ¹¹Center for Frontier Science, Chiba University, 1-33 Yayoi-cho, Inage-ku, Chiba 263-8522, Japan; ¹²Department of Astronomy, School of Science, SOKENDAI (The Graduate University for Advanced Studies), 2-21-1 Osawa, Mitaka, Tokyo 181-8588, Japan; ¹³National Astronomical Observatory of Japan, 2-21-1 Osawa, Mitaka, Tokyo 181-8588, Japan; ¹⁴Division of Particle and Astrophysical Science, Nagoya University, Furo-cho, Chikusa-ku, Nagoya 464-8602, Japan; ¹⁵The Research Center for Statistical Machine Learning, The Institute of Statistical Mathematics, 10-3 Midori-cho, Tachikawa, Tokyo 190-8562, Japan; ¹⁶Institute for Advanced Research, Nagoya University, Furo-cho, Chikusa, Nagoya 464-8602, Japan; ¹⁷Department of Physics, Graduate School of Science, Nagoya University, Furocho, Chikusa, Nagoya 464-8602, Japan;

Accreting supermassive black holes (SMBHs) are thought to influence the evolution of their host galaxies through multi-phase feedback driven by powerful nuclear outflows^{1,2}. Although this mechanism is central to theoretical models of SMBH–galaxy co-evolution across cosmic time³, direct observational evidence connecting nuclear winds to large-scale cold gas outflows remains limited, especially in the early universe. Here we report statistical evidence for such a connection in a sample of luminous quasars at $z \sim 5.5$. We compare stacked [C II] 158 μm emission profiles from ALMA observations, which trace galactic-scale neutral gas, for quasars with and without broad absorption lines (BALs) that indicate powerful nuclear winds on sub-kiloparsec scales⁴. The BAL quasar stack exhibits a signif-

icant ($S/N = 4.45$) blueshifted broad component in the [C II] line profile, with a velocity offset of $\Delta v_b = -2.1 \times 10^2 \text{ km s}^{-1}$ and a full width at half maximum of $1.18 \times 10^3 \text{ km s}^{-1}$, whereas the non-BAL stack shows no such feature. We estimate that a few percent to one-quarter of the nuclear wind energy may be transferred to cold neutral gas on kiloparsec scales. These results suggest that BAL winds can couple to the host galaxy’s interstellar medium, providing empirical support for models of multi-phase AGN feedback^{5,6}. This mechanism may also contribute to the observed diversity in M_{BH}/M_* among luminous quasars recently identified by JWST^{7,8}.

1 Introduction

Quasars are powered by accretion onto supermassive black holes (SMBHs). Understanding whether and how quasars impact their host galaxies is crucial for investigating the co-evolution of SMBHs and galaxies^{1,2}, particularly in the early universe. In this context, it is essential to study how physics in the nuclear region influences the interstellar medium (ISM) on galactic scales.

The [C II] 158 μm fine-structure line is one of the strongest cooling lines of the ISM and serves as a key tracer of both star formation and gas dynamics^{9–11}. It provides insights into the properties of the cold ISM, typically at temperatures of $T \sim 10^2\text{--}10^3 \text{ K}$, and has been extensively used in studies of galaxies across cosmic time^{12,13}. Broad wings in the [C II] line profile have been interpreted as signatures of large-scale outflows driven by AGN or intense star formation^{5,14}. However, recent re-analyses using deeper and wider-bandwidth data have questioned the statistical significance of such features in some individual systems¹⁵. Moreover, star formation alone can also drive detectable [C II] wings, even in the absence of AGN activity, as shown in both stacked and individual high-redshift galaxies^{16–20}. These findings underscore the complexity of interpreting broad [C II] profiles and highlight the importance of carefully distinguishing between AGN- and star formation-driven feedback in population-level analyses.

Recent studies have explored whether [C II] outflows correlate with quasar properties such as luminosity or black hole accretion rate. Stacking analyses of $z > 6$ quasars have so far found limited evidence for outflow features in [C II] emission^{21–23}, while other works report more extended or kinematically

[†]Email: yongdaz@arizona.edu

disturbed [C II] components in selected individual quasars^{24–26}. These conflicting results suggest that detecting outflows using [C II] alone is nontrivial and may depend sensitively on sample properties, spatial resolution, and stacking methodology.

An effective tracer of nuclear winds is the presence of broad absorption line (BAL) features in quasar spectra. BALs are associated with high-velocity outflows launched near the accretion disk and are observed in a significant fraction of luminous quasars^{4,27,28}. These outflows can reach velocities of thousands of kilometers per second and are thought to originate from radiation-driven winds in the nuclear region²⁹.³⁰ reported that the fraction of BAL quasars increases toward higher redshift (e.g., in the XQR-30 program;³¹), implying that nuclear winds may be more prevalent or visible during the reionization epoch. Investigating whether such small-scale winds are physically connected to larger-scale gas dynamics is crucial for understanding early SMBH–galaxy co-evolution. This is particularly relevant given recent evidence that some luminous quasars deviate from the local $M_{\text{BH}}-M_*$ relation⁸.

In this work, we investigate this connection using a sample of 17 quasars (16 used for stacking) at $z \sim 5.5$, near the end of reionization^{32,33}. Our observations, conducted with ALMA and Keck/ESI, enable a consistent comparison between BAL and non-BAL quasars. By stacking the [C II] profiles, we find that the BAL sample exhibits a statistically significant broad wing component not seen in the non-BAL stack. While this result suggests a potential coupling between nuclear and large-scale cold gas outflows, we interpret it in the context of existing uncertainties and complementary scenarios, including star formation-driven winds and orientation effects.

This paper is organized as follows. In Section 2, we describe the ALMA [C II] observations and Keck/ESI spectra of our quasar sample. Section 3 presents the main results of our [C II] profile analysis. In Section 4, we discuss the implications of our findings, and we summarize our conclusions in Section 5. Throughout this paper, we adopt the Planck18 cosmology³⁴, implemented in *astropy*³⁵. All distances are quoted in proper units unless otherwise noted.

2 Data

We use the brightest quasars in the z -band ($m_z \lesssim 20$) selected by Yang et al.^{36,37}, identified through a systematic search for high-redshift quasars. These quasars fill the so-called “redshift gap” at $z \sim 5.5$, a regime that was historically underrepresented in quasar surveys due to color degeneracy with brown dwarfs in broadband photometry. Yang et al. overcame this challenge by incorporating additional Y -band imaging to break the degeneracy, enabling us to investigate quasar properties in this key transitional epoch near the end of cosmic reionization.

2.1 ALMA Observations In Cycle 9 (2022.1.00662.S; PI: Zhu), we conducted ALMA Band 7 observations targeting 21 quasars at $z \sim 5.5$ from^{36,37}, aiming to determine precise systemic redshifts ($\Delta z \sim 10^{-4}$) through [C II] 158 μm emission (details in³⁸). Each observation employed two overlapping spectral windows fully covering the [C II] line at the expected redshift, alongside two additional spectral windows for

dust continuum measurements. The observations used the C43- (1, 2, and 3) configurations, achieving an angular resolution of $\sim 1''$ across the entire sample.

Data calibration and reduction were performed using the CASA pipeline (version 6.4.1.12;^{39,40}). We generated data cubes and imaged the [C II] emission following procedures outlined in⁴¹. Continuum subtraction was conducted in the uv -domain using all line-free channels across the four spectral windows by fitting a first-order polynomial. Imaging was performed with *tclean*, using natural weighting to optimize sensitivity. The average RMS noise level across the dataset is $\sim 0.25 \text{ mJy beam}^{-1}$ per 30 MHz bin.

Spectra were extracted using a single-beam aperture centered on each source to minimize contamination from extended [C II] emission and complex host galaxy kinematics. To evaluate the impact of aperture size, we also tested extractions using a standard 2-beam diameter aperture. For the BAL quasar stack, the broad wing detection significance decreased from 4.45 (Section 3) to 3.3σ , while for the non-BAL stack, it dropped from $<2\sigma$ to below 1.5σ . Although a larger aperture introduces increased noise, the decrease in S/N for the BAL stack exceeds what is expected from noise alone, suggesting that physical dilution (via inclusion of unrelated kinematic components) is the dominant factor. This supports our choice of using the single-beam aperture for the fiducial analysis.

We include only quasars with successful [C II] detections. Three quasars — J0157+3001, J1420-1602, and J1527+0641 — are excluded because the [C II] line may fall outside the spectral coverage. Additionally, J1133+1603 is excluded due to its close companion exhibiting a [C II] bridge suggesting interaction and complex gas kinematics⁴². The final ALMA sample comprises 17 quasars. The resulting [C II] images and spectra are presented in Figure 1. We determined the systemic redshift for each quasar by fitting a Gaussian profile to the [C II] emission line.

2.2 ESI Spectra We acquired the Keck/ESI spectra for most quasars in this sample, which we use to identify BAL features in the rest frame UV. We conducted ESI observations for 13 quasars between 2021 and 2024 and retrieved archival spectra for one additional quasar. For the remaining three (J1006, J1048, and J1614), we used existing confirmation spectra from^{36,37}, obtained with SSO-2.3m/WiFeS^{43,44} and Palomar-200-inch (P200)/DBSP.

The data were reduced using a custom IDL/GDL⁴⁵ pipeline, following procedures described in⁴⁶ and³⁸. This pipeline incorporates optimal sky subtraction techniques⁴⁷, one-dimensional spectral extraction⁴⁸, and telluric absorption corrections based on the Cerro Paranal Advanced Sky Model^{49,50}. The extracted spectra have a pixel size of 15 km s^{-1} , with a typical velocity resolution of approximately 45 km s^{-1} (FWHM). The signal-to-noise ratio (S/N) per 30 km s^{-1} bin is greater than 10 near 1285 Å in the rest frame.

In this work, we focus on quasars with BAL outflows, i.e., classic BAL quasars, defined by a balnicity index $\text{BI}_0 > 0 \text{ km s}^{-1}$ ^{4,51}. The balnicity index is computed using the equation:

Table 1 – Quasar Sample Used in This Work

No.	Quasar	RA (J2000)	Dec (J2000)	$z_{[\text{CII}]}$	M_{1450}	BI_0 (km s $^{-1}$)	ESI
1	J0012+3632	00:12:32.88	+36:32:16.10	5.485 ± 0.001	-27.2	5650.9	2021-10
2	J0056+2241 ^a	00:56:56.04	+22:41:12.16	5.5218 ± 0.0002	-26.8	0.0	2022-09
3	J0120+2147	01:20:53.92	+21:47:06.20	5.4305 ± 0.0001	-26.5	0.0	2023-09
4	J0231-0728	02:31:37.64	-07:28:54.44	5.4227 ± 0.0005	-26.6	0.0	2013-01
5	J0306+1853	03:06:42.51	+18:53:15.85	5.3808 ± 0.0001	-28.9	0.0	2021-10
6	J1006-0310 ^b	10:06:14.61	-03:10:30.49	5.5149 ± 0.0004	-27.0	0.0	-
7	J1016+2541	10:16:37.70	+25:41:31.98	5.6797 ± 0.0004	-27.7	471.8	2024-06
8	J1022+2252	10:22:10.04	+22:52:25.44	5.4787 ± 0.0005	-27.3	1501.9	2016-03
9	J1048+3339 ^c	10:48:36.72	+33:39:47.66	5.6219 ± 0.0002	-27.0	0.0	-
10	J1335-0328	13:35:56.23	-03:28:38.20	5.699 ± 0.004	-27.8	304.8	2024-05
11	J1500+2816	15:00:36.83	+28:16:03.03	5.5727 ± 0.0006	-27.6	0.0	2024-06
12	J1513+0854	15:13:39.64	+08:54:06.58	5.4805 ± 0.0003	-26.8	0.0	2021-05
13	J1614+0114 ^c	16:14:35.35	+01:14:44.79	5.7945 ± 0.0004	-26.9	0.0	-
14	J1650+1617	16:50:42.25	+16:17:21.50	5.5769 ± 0.0001	-27.2	477.7	2021-05
15	J2207-0416	22:07:10.12	-04:16:56.28	5.5297 ± 0.0003	-27.8	2447.0	2021-10
16	J2317+2244	23:17:38.25	+22:44:09.63	5.558 ± 0.0002	-27.4	4329.0	2022-09
17	J2325+2628	23:25:14.24	+26:28:47.61	5.7514 ± 0.0001	-27.0	2676.2	2021-10

Notes: Columns: (1) Index; (2) quasar name; (3) and (4) quasar coordinates (J2000); (5) [C II] redshift; (6) absolute magnitude at rest-frame 1450 Å, based on quasar luminosities from ^{36–38}; (7) balnicity, where strong BAL quasars ($\text{BI}_0 > 1000$ km s $^{-1}$; see text for details) are marked in bold; (8) date of the most recent Keck/ESI observation.

^a Outflow signature shown in the [CII] image.

^b See ³⁶ for spectra.

^c See ³⁷ for spectra.

$$\text{BI}_0 = \int_{v_{\min}}^{v_{\max}} \left(1 - \frac{f(v)}{0.9}\right) C(v) dv, \quad (1)$$

where $f(v)$ is the normalized flux as a function of velocity, $C(v)$ is a continuity function equal to 1 when absorption depth exceeds 10% over at least 2000 km s $^{-1}$, and 0 otherwise. We adopt $v_{\min} = 0$ km s $^{-1}$ and $v_{\max} = 64500$ km s $^{-1}$ ³⁰.

We set zero velocity at C IV and identify BALs in both Si IV and C IV. Due to incomplete wavelength coverage, we do not attempt precise BI_0 measurements. A major source of uncertainty in computing BI_0 is the power-law continuum fitting. Three quasars (J1006, J1048, J1650) yield $\text{BI}_0 > 0$, but their BAL features are not visually apparent and may be influenced by telluric absorption or noise near spectral edges. To ensure robustness, we classify only quasars with significant BAL features ($\text{BI}_0 > 1000$ km s $^{-1}$) as BAL quasars. We identify five quasars meeting this criterion. Among our sample, J0012, J2317, and J2325 exhibit the most unambiguous BAL features ($\text{BI}_0 > 2500$ km s $^{-1}$). As a consistency check, stacking [C II] emission for these three quasars alone yields a significant ($> 3\sigma$) broad [C II] wing (Section 3).

To compute $f(v)$, we normalized observed fluxes by fitting a power-law continuum to each quasar spectrum in the rest-frame wavelength range of 1285–1450 Å, masking strong emission or absorption lines. Figure 2 displays all ESI spectra, continuum fits, and BAL identifications. The detailed properties of our quasar sample are summarized in Table 1.

3 Stacked [C II] Spectra

We create stacked [C II] spectra for the five strong BAL quasars and eleven non-BAL quasars, respectively. The quasar J0056+2241 is excluded from both stacks due to its independently identified strong and extended [C II] feature in the emission line map. To construct the stacks, we normalize each spectrum by its peak flux, shift the [C II] emission line to the systemic redshift, and compute the mean stack in velocity space (Δv — the velocity offset relative to the systemic redshift) using bins of 60 km s $^{-1}$. The spectra are weighted by their inverse variance, although we verified that not weighting by inverse variance does not change the results, given the relatively consistent rms level across the entire quasar sample. We perform 1,000 bootstrap resamplings (with replacement) of 5 spectra from the BAL sample and 11 spectra from the non-BAL sample, respectively, to estimate the variance in the stacked profiles.

For the stacked spectra, we find that a single Gaussian profile centered at $\Delta v = 0$ cannot adequately describe the signal, especially for the BAL stack. Therefore, we fit a two-component Gaussian model: a narrow component with velocity dispersion $\sigma < 500$ km s $^{-1}$ and a broad component with $\sigma > 500$ km s $^{-1}$. The narrow component’s line center is fixed at $\Delta v = 0$, while the broad component’s center is allowed to vary. We derive uncertainties in the fit parameters based on the stacked fluxes across the bootstrap realizations.

Figure 3 panels (a) and (b) present the stacked [C II] profiles for the BAL and non-BAL samples, respectively. In the BAL stack, a single narrow Gaussian cannot fully explain the

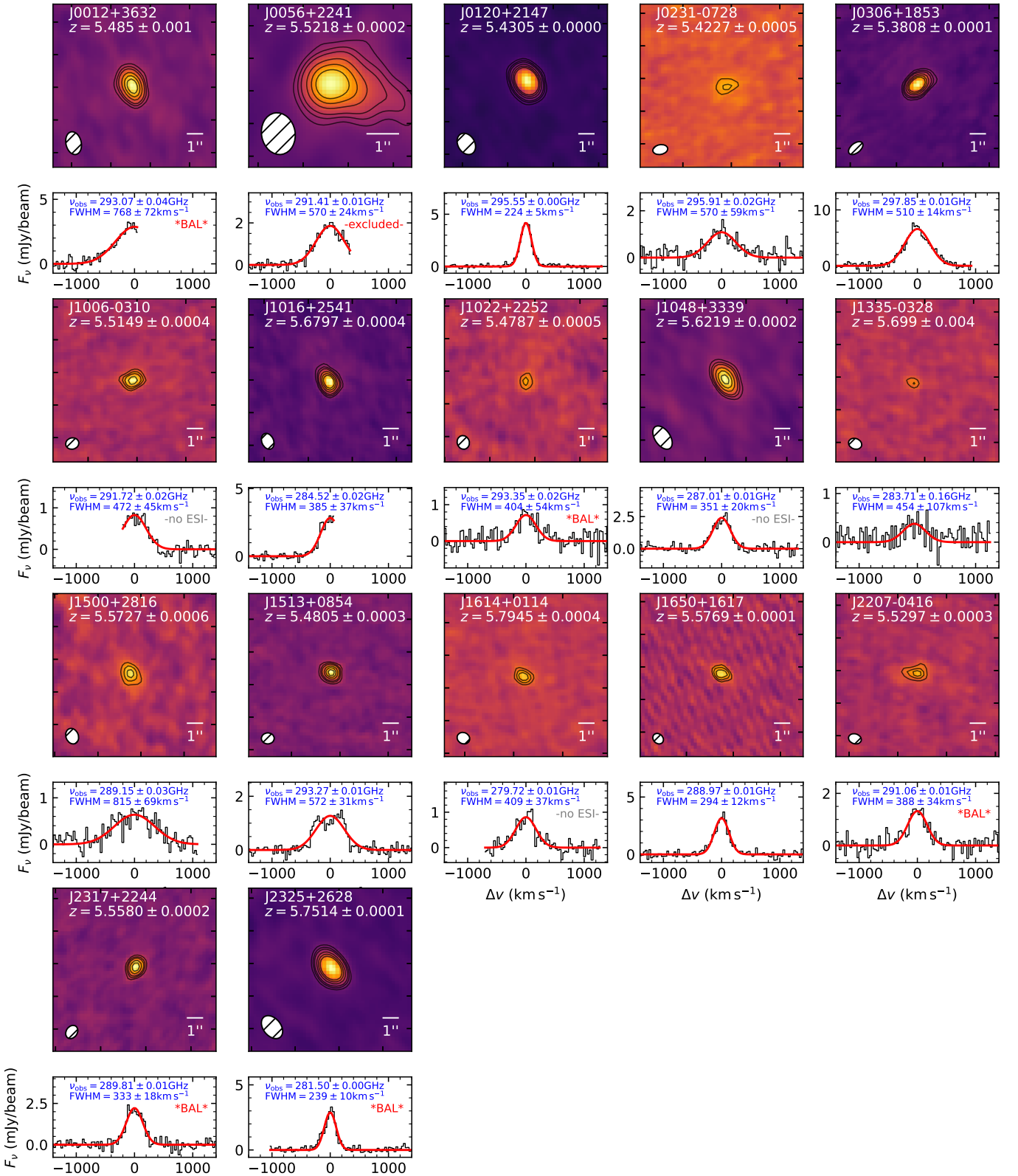


Figure 1 – [C II] 158μm emission maps and spectra of the quasar sample observed with ALMA. Contours show (2σ , 3σ , 4σ , 6σ , 8σ , 10σ) levels. The synthesized beam is shown in the lower-left corner of each map. Measured redshifts are labeled for each quasar and red curves show the best Gaussian fits. Observed frequency and FWHM of the [C II] emission are also provided for reference. Quasars with significant BAL features are labeled, while those without ESI spectra are marked as “no ESI”. Since J0056 exhibits very extended [C II] emission in the image, it has been excluded from the stacking analysis.

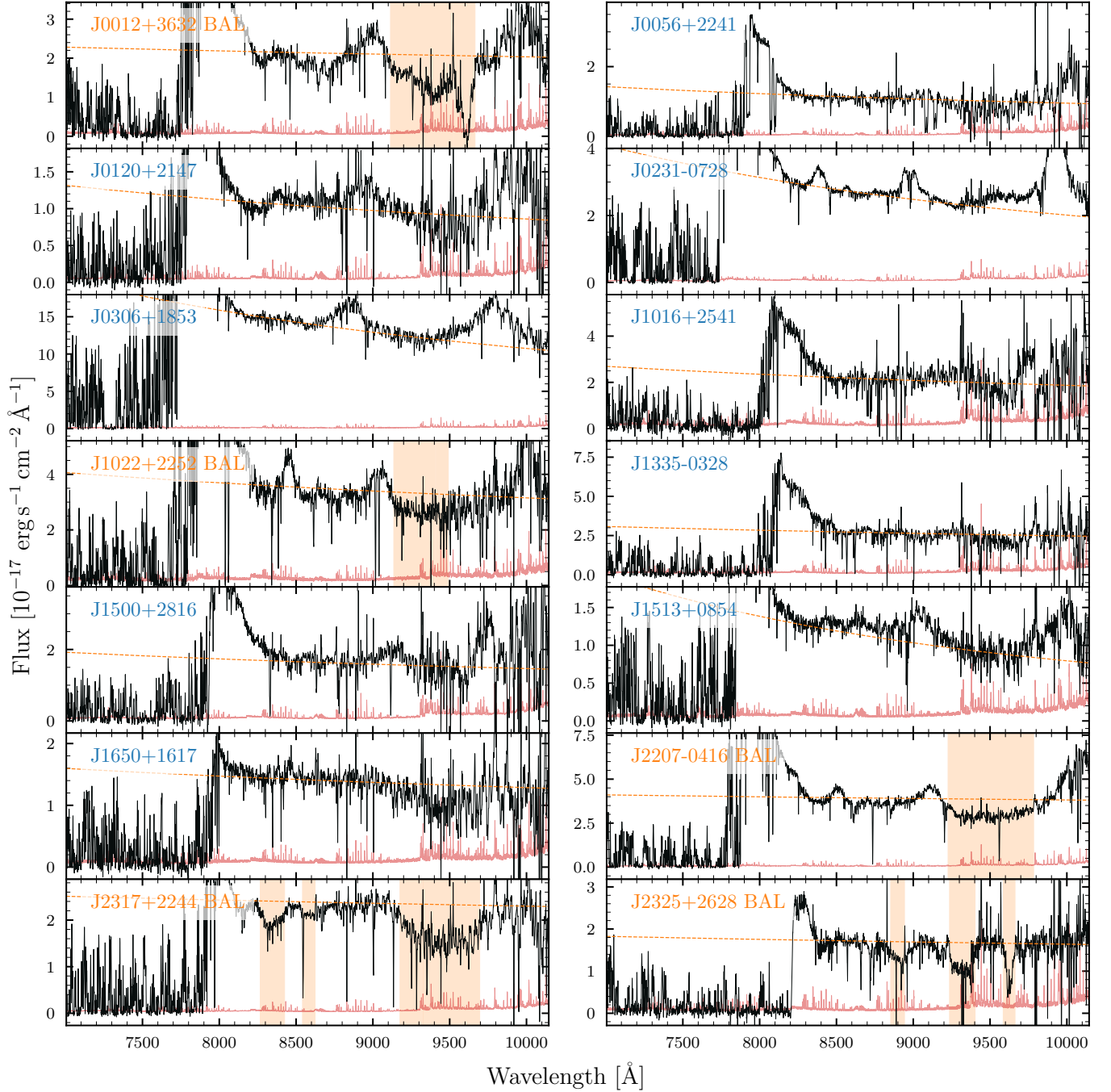


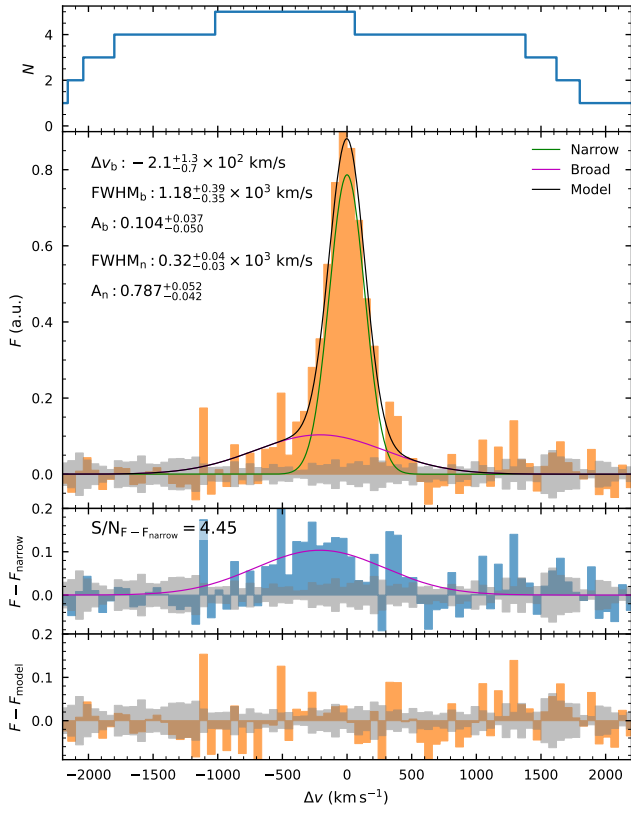
Figure 2 – Keck/ESI rest-frame UV spectra of the quasar sample. Black and red colors plot the flux and corresponding error array, respectively. BAL quasars ($BI_0 > 1000 \text{ km s}^{-1}$) are labeled with orange text, and regions shaded in orange highlight prominent BAL absorption troughs. The dashed curves indicate the power-law continuum fits used to normalize the spectra.

observed profile due to the presence of a significant blueshifted broad component. The residual broad emission is detected with a mean signal-to-noise ratio of 4.45 within its FWHM (i.e., a 4.45σ detection). The best-fit Gaussian for the broad component yields a line center at $\Delta v_b = -2.1^{+1.3}_{-0.7} \times 10^2 \text{ km s}^{-1}$

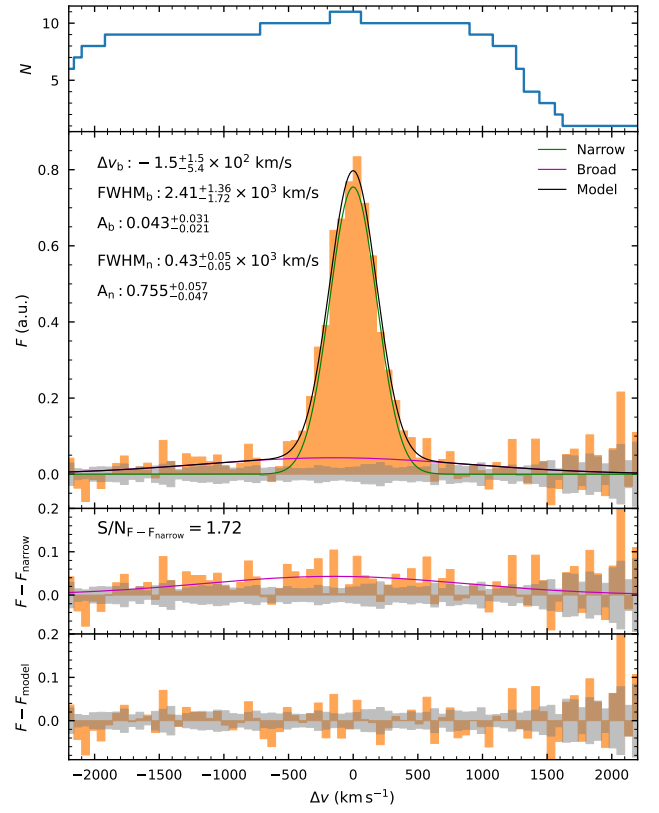
However, the σ value quoted here represents the signal detection level rather than a strict statistical significance, as there remains a $\lesssim 2\%$ probability that a stack of five non-BAL quasars could yield a similar broad component detection (see Section 4 and Figure A2).

and a FWHM of $1.18^{+0.39}_{-0.35} \times 10^3 \text{ km s}^{-1}$. We revisit the individual spectra in Figure 1 and notice that some BAL quasars show a slight gradual decrease in the flux toward the bottom of their single Gaussian fit; however, these features are too noisy to make robust measurements individually (e.g., J0012 and J2325). Nevertheless, these features become prominent in the stacked spectrum.

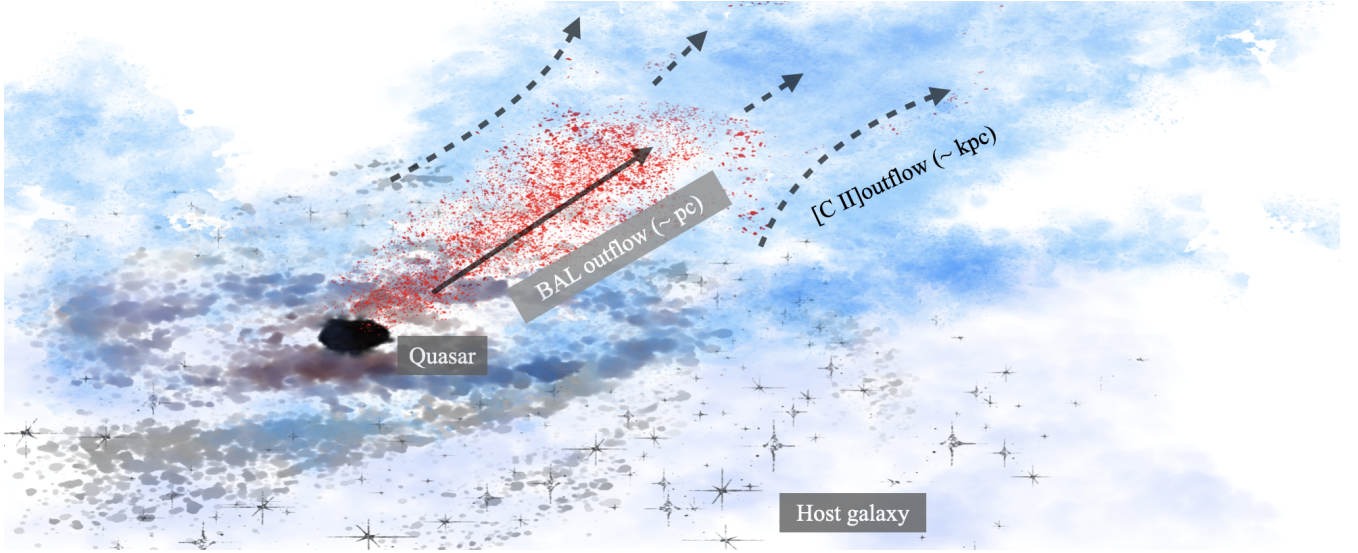
In contrast, the non-BAL stack does not exhibit a significant broad component, and the broad residual has a detection sig-



(a) BAL stack



(b) non-BAL stack



(c)

Figure 3 – Stacked [C II] spectra and an illustration of quasar-driven outflows. **(a)** Stacked [C II] profile for the BAL quasar sample. The top panel shows the number of spectra contributing to the stack at each velocity bin (Δv). The middle panel displays the normalized [C II] flux, with the best-fit narrow (green) and broad (cyan) Gaussian components. The combined model is shown in black, with a broad component centered at $\Delta v_b = -2.1 \times 10^2 \text{ km s}^{-1}$ and a FWHM of $1.18 \times 10^3 \text{ km s}^{-1}$. The residuals between the total flux and the narrow component are shown in the third panel, highlighting the significance of the broad residual (mean $S/N = 4.45$ within the FWHM). The bottom panel shows the overall residuals after subtracting the total model. **(b)** Stacked [C II] profile for the non-BAL quasar sample. The profile lacks a significant broad component, with residuals below 2σ . **(c)** A conceptual illustration of quasar outflows. The red region represents nuclear outflows traced by the BAL phase, while the diffuse blue region illustrates large-scale cold gas outflows traced by [C II]. This plot, not to physical scale, depicts the potential coupling between small-scale nuclear winds and galactic-scale outflows. The artwork was created by Y. Zhu using Adobe Fresco.

nificance below 2σ . The Gaussian fit for the broad component is unconstrained. We note that the noise level in the non-BAL stack is lower than in the BAL stack due to the larger sample size. This reinforces the indication that the large-scale outflows traced by [C II] are predominantly associated with BAL quasars in our sample.

Additionally, we note that the narrow component of the BAL stack is narrower ($\text{FWHM} = 3.2 \times 10^2 \text{ km s}^{-1}$) than that of the non-BAL case ($\text{FWHM} = 4.3 \times 10^2 \text{ km s}^{-1}$). This difference might be attributed to viewing angle effects (see Section 4).

4 Discussion

4.1 Nuclear Winds and the Origin of the [C II] Wing The observed association between [C II] outflows and BAL quasars may reflect direct coupling between parsec-scale nuclear winds and galactic-scale cold gas. Multi-phase simulations predict such coupling⁵², and our stacking analysis provides statistical evidence for its occurrence at high redshift. Figure 3(c) illustrates the proposed scenario: if the BAL outflow axis aligns with our line of sight, we observe blueshifted broad absorption features in high-ionization UV lines (e.g., C IV, Si IV) and, on kiloparsec scales, blueshifted [C II] emission tracing the entrained neutral ISM. In contrast, non-BAL quasars, either lacking strong nuclear winds or viewed from different sightlines, may show narrower or no blueshifted [C II] wings. The narrower width of the [C II] narrow component in the BAL stack ($\text{FWHM} = 3.2 \times 10^2 \text{ km s}^{-1}$) compared to the non-BAL stack ($\text{FWHM} = 4.3 \times 10^2 \text{ km s}^{-1}$) is consistent with a more face-on orientation, while broader [C II] lines in non-BALs likely reflect complex rotational and dynamical structures viewed closer to edge-on.

Alternative interpretations must be considered. First, galaxy mergers or unresolved companion galaxies may broaden [C II] profiles or introduce asymmetric wings. Although our sample excludes obvious companions in the ALMA cubes, higher-resolution observations would be needed to fully rule out blended structures. Second, star formation-driven outflows are known to contribute to [C II] wings, even in non-AGN systems^{16–20}. Since quasars often reside in star-forming galaxies, some [C II] broad emission may arise from stellar feedback rather than AGN winds. However, if star formation were the dominant cause, we would expect comparable [C II] wings in the non-BAL sample, which we do not observe. Still, we caution that our stacking analysis cannot unambiguously disentangle AGN- and star formation-driven outflows. The energetics discussed below therefore represent upper limits on AGN coupling efficiency, assuming the [C II] broad component is primarily AGN-driven.

Third, orientation effects likely play a significant role. BALs are preferentially observed along sightlines aligned with the nuclear wind axis²⁹, and large-scale outflows, whether AGN- or star formation-driven, are expected to emerge perpendicular to the galactic plane. This implies a potential geometric alignment bias: face-on systems are more likely to show both BAL features and outflow signatures in integrated spectra. The narrower [C II] profiles in BAL quasars further support this orientation scenario. However, disk–AGN alignment is not guaranteed and may vary across systems⁵³. The observed trend could also arise from structural alignment between the quasar outflow axis and the

host disk normal. A more complete treatment of orientation and multiphase outflows will require spatially resolved data, ideally combining [C II], ionized gas, and stellar continuum mapping.

While our results may support a connection between BAL winds and kiloparsec-scale cold gas outflows, we stress that other mechanisms—including star formation feedback, minor mergers, and viewing angle—likely contribute. A definitive causal link between nuclear winds and [C II] broad wings will require larger samples and spatially resolved observations to isolate these effects.

4.2 Energetics and Coupling Efficiency Between BAL and Cold Gas Outflows To quantify the potential coupling between nuclear and cold gas outflows, we estimate the kinetic power of each phase. For the BAL outflows, we adopt a hydrogen column density of $N_{\text{H}} = 10^{20.1 \sim 22.6} \text{ cm}^{-2}$ ⁵⁴ and outflow radii $\log_{10}(R_{\text{out}}/\text{pc}) = 0 \sim 2$ ^{24,55,56}. With a mean velocity offset of the broad absorption troughs of $v_{\text{BAL}} = 2.5 \times 10^4 \text{ km s}^{-1}$ and assuming covering fraction of $f_{\text{cov}} = 0.2$ ⁵⁷, the mass outflow rate is

$$\dot{M}_{\text{BAL}} = 4\pi R_{\text{out}} N_{\text{H}} \mu m_{\text{p}} f_{\text{cov}} v_{\text{BAL}}, \quad (2)$$

where $\mu = 1.4$ accounts for helium. The corresponding kinetic power is

$$\dot{E}_{\text{BAL}} = \frac{1}{2} \dot{M}_{\text{BAL}} v_{\text{BAL}}^2 \approx 10^{44.3-46.3} \text{ erg s}^{-1}. \quad (3)$$

For the [C II] outflow, we adopt an outflow radius of 3.0 kpc, matching the mean ALMA beam size and consistent with the measurements in⁵⁸. The fraction of the flux in the broad component over the total stacked flux is $F_{\text{broad}}/F_{\text{total}} = 0.32 \pm 0.11$. The outflow velocity is computed in the standard way following e.g.,⁵⁸:

$$v_{[\text{CII}]} = |\Delta v_{\text{b}}| + \frac{\text{FWHM}_{\text{broad}}}{2} = (8.0 \pm 2.1) \times 10^2 \text{ km s}^{-1}. \quad (4)$$

Following⁵⁹, the outflow mass is given by

$$M_{\text{out}}/M_{\odot} = 0.77 \left(\frac{0.7 L_{[\text{CII}]}}{L_{\odot}} \right) \left(\frac{1.4 \times 10^{-4}}{X_{\text{C}^{+}}} \right) \times \frac{1 + 2e^{-91K/T} + n_{\text{crit}}/n}{2e^{-91K/T}}, \quad (5)$$

where $L_{[\text{CII}]}$ is the [C II] luminosity of the broad component determined by $F_{\text{broad}}/F_{\text{total}}$, $n_{\text{crit}} \sim 3 \times 10^3 \text{ cm}^{-3}$ is the critical density, and $X_{\text{C}^{+}} = 10^{-4}$ is the assumed abundance of C^{+} ^{5,58}. Assuming $n \gg n_{\text{crit}}$ and a temperature range of $T \sim 100\text{--}1000 \text{ K}$, we obtain a mean outflow mass of $M_{\text{out}} = (9.3 \pm 0.2) \times 10^8 M_{\odot}$.

The time-averaged mass outflow rate is then given by

$$\dot{M}_{\text{out}} = \frac{v_{[\text{CII}]} \times M_{\text{out}}}{R_{\text{out}}} \approx 10^{2.3-2.4} M_{\odot} \text{ yr}^{-1}, \quad (6)$$

and the kinetic power by

$$\dot{E}_{\text{out}} = \frac{1}{2} \dot{M}_{\text{out}} \times v_{[\text{C II}]}^2 \approx 10^{43.6-43.8} \text{ erg s}^{-1}. \quad (7)$$

Finally, the coupling efficiency between the BAL and [C II] outflows is

$$\eta = \frac{\dot{E}_{\text{out}}}{\dot{E}_{\text{BAL}}} = 0.025^{+0.23}_{-0.022}. \quad (8)$$

The inferred coupling efficiency suggests that BAL winds can transfer a non-negligible fraction, ranging from a few percent up to one-quarter, of their kinetic energy into large-scale neutral gas outflows. However, this estimate relies on several simplified assumptions. The intrinsic properties of BAL winds, such as column density, launch radius, and covering fraction, vary substantially across studies^{6,60}. Moreover, the physical scales involved are distinct: BAL winds originate in the nuclear region on sub-kiloparsec scales, while [C II] emission traces cold gas on kiloparsec scales. As a result, any direct energy comparison between the two phases remains uncertain. The [C II] outflow may represent only the cold, neutral component of a broader multiphase outflow, and the inferred energetics likely provide a lower limit on the total energy transferred by nuclear winds. Furthermore, since [C II] traces relatively long-lived gas, the observed broad component may reflect the cumulative effects of past BAL phases rather than strictly ongoing nuclear activity.

As a conservative estimate, the cold gas mass outflow rate is approximately $10^2 M_{\odot} \text{ yr}^{-1}$. If the host galaxies had masses similar to the Milky Way (though this is likely an overestimate), the escape velocity at a galactocentric radius of 1 kpc would be about 700 km s^{-1} ^{61,62}. Our measured outflow velocity is $\sim 800 \text{ km s}^{-1}$, suggesting that the gas is capable of escaping the host potential well. For a typical quasar with $\log(L_{[\text{C II}]} / L_{\odot}) \sim 9$, corresponding to a star formation rate of $\log(\text{SFR}) \sim 2$ ¹¹, the cold gas outflow rate is comparable to the ongoing star formation. If a significant fraction of this gas is permanently expelled or remains unavailable for star formation on short timescales, the depletion of the cold gas reservoir could suppress future star formation. However, fully assessing the long-term impact of such outflows requires additional constraints on gas recycling, accretion, and the quasar duty cycle.

Given the high BAL fraction among luminous quasars at $z \gtrsim 5.5$ (approximately 50%;³⁰) and the statistical link between BALs and [C II] outflows shown here, this mechanism may play a role in regulating the cold gas supply and shaping SMBH–galaxy co-evolution. Some high-redshift quasars exhibit elevated M_{BH} / M_{*} ratios relative to the local Magorrian relation, though these deviations can be explained by rapid black hole growth, delayed stellar mass assembly, or selection biases, rather than requiring systematically overmassive black holes⁸. The role of BAL-driven feedback remains uncertain, as recent observations also suggest that star formation can be enhanced in some quasar hosts⁶³. A more nuanced view of quasar–galaxy interplay, including time variability and environmental effects, will be essential to interpreting these results in a broader evolutionary framework.

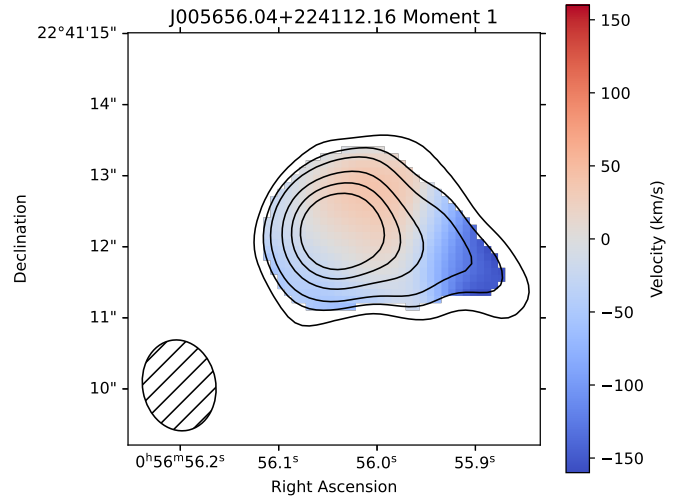


Figure 4 – The moment 1 (velocity) map of J0056+2241 relative to its systemic redshift of $z = 5.5218$. The contours represent significance levels of (2σ , 3σ , 4σ , 6σ , 8σ , 10σ) from the moment 0 map. The map reveals blueshifted emission within the extended [C II] structure, although the velocity remains within the FWHM of its emission line profile, as shown in Figure 1.

4.3 Individual Quasar: J0056+2241 Among our quasar sample, the non-BAL quasar J0056+2241 exhibits an exceptionally extended morphology in its [C II] emission map, with a tail extending over $2''.5$ (corresponding to $\sim 15 \text{ kpc}$) toward the southwest from the quasar center. The moment 1 map (Figure 4) reveals blueshifted emission within the extended [C II] structure, with a velocity offset of ~ -100 – 150 km s^{-1} , although this velocity remains within the width of its emission line profile ($\text{FWHM} = 570 \text{ km s}^{-1}$; Figure 1). This large-scale structure may indicate a significant outflow of cold gas on galactic scales, possibly driven by strong AGN activity. However, such an extended structure could also result from other processes, such as a merger^{64,65}.

Interestingly, despite this potential morphological evidence of outflows, the ESI spectrum of J0056+2241 does not show strong BAL features. However, there is a notable flux discontinuity redward of the $\text{Ly}\alpha + [\text{N V}]$ emission complex. Additionally, the $\text{Ly}\alpha$ line itself is associated with strong absorption features, as also noted in³⁸. These absorbers may indicate the presence of intervening gas clouds or infalling material along the line of sight.

One potential explanation for the lack of BAL features is that the outflows in J0056+2241 may not be well-aligned with our line of sight. Indeed, we do not see strong blueshifted [C II] emission, suggesting that the [C II] outflow is also not aligned along our line of sight. In this scenario, the outflow may be oriented at an angle where high-velocity winds do not produce strong absorption features in the rest-frame UV spectrum. Alternatively, the outflow may be dominated by dense, neutral gas phases that are less effective at producing BAL signatures in high-ionization species such as C IV and Si IV.

Another possibility is a difference in timescales between nuclear and galactic-scale outflows. If the large-scale outflow

observed in [C II] is a remnant of past AGN activity, the current nuclear wind may no longer be strong enough to produce detectable BAL features in the UV. Alternatively, J0056+2241 may be in an early stage of outflow development, where neutral gas has already been accelerated to large scales, but the ionized phase has not yet fully developed. Further spatially resolved spectroscopic observations, particularly in ionized and molecular gas tracers, could help disentangle the structure and dynamics of the outflow in J0056+2241, providing additional insight into the feedback mechanisms in this system.

Finally, as a sanity check, including J0056+2241 in our non-BAL quasar stack increases the significance of the broad component only from 1.72σ to 1.77σ , which is slightly higher than when excluding J0056+2241. This suggests that its extended [C II] emission may contribute modestly to the overall broad wing detected in the stacked profile.

5 Summary

We present evidence for a potential connection between nuclear winds and large-scale cold gas outflows in high-redshift ($z \sim 5.5$) quasars, based on a stacking analysis of ALMA [C II] $158 \mu\text{m}$ emission line profiles in BAL and non-BAL subsamples. Our main findings are:

1. The stacked [C II] spectrum for BAL quasars reveals a significant blueshifted broad component, with a velocity offset of $\Delta v_b = -2.1 \times 10^2 \text{ km s}^{-1}$ and a FWHM of $1.18 \times 10^3 \text{ km s}^{-1}$, consistent with large-scale cold gas outflows. The non-BAL stack shows no statistically significant broad component. While this difference may reflect a physical link between BAL winds and cold gas outflows, alternative explanations such as galaxy orientation or differing host properties cannot be excluded.
2. We estimate a coupling efficiency of $\eta = 0.025^{+0.23}_{-0.022}$ between the kinetic power of BAL outflows and that of the [C II]-traced outflows. This suggests that BAL winds may transfer a non-negligible fraction of their energy into neutral gas on kiloparsec scales. However, this estimate assumes that the [C II] broad component is AGN-driven; contributions from star formation-driven winds would reduce the inferred efficiency.
3. The non-BAL quasar J0056+2241 displays an extended [C II] tail spanning $\sim 15 \text{ kpc}$ with blueshifted emission, suggestive of an outflow or merger-induced disturbance. Despite lacking strong BAL features, its morphology implies that orientation, feedback history, or merging activity may play a role in shaping large-scale gas dynamics.

Taken together, our results support a scenario in which nuclear outflows may contribute to cold gas removal in quasar host galaxies during the reionization epoch. Nonetheless, the interpretation is limited by sample size, uncertainties in star formation contributions, and potential orientation biases. Further spatially resolved, multi-phase observations will be essential to robustly constrain the physical origin of [C II] wings and the role of BAL winds in early feedback processes. If confirmed with a larger sample, given the high BAL incidence at $z > 5$ ³⁰, such

winds may be a key component of AGN–host co-evolution at the end of reionization.

Methods

Intrinsic Properties of Quasars and Sample Size Here, we discuss potential systematics and caveats that could influence our results. Previous studies have found a positive correlation between the incidence of [C II] outflows and quasar bolometric luminosity, suggesting that more luminous quasars are more likely to drive large-scale outflows^{5,58}. Since direct measurements of bolometric luminosity are not available for our sample, we use M_{1450} as a proxy, assuming a typical bolometric correction for high-redshift quasars. Figure A1 shows the distribution of our quasar sample in the M_{1450} versus redshift plane. Our sample spans a narrow redshift range, and both BAL and non-BAL quasars exhibit similar distributions in M_{1450} . This similarity reduces the likelihood that luminosity-related biases are responsible for the observed differences in [C II] profiles between the two samples.

To test whether the observed broad [C II] wing is driven by brighter quasars that preferentially exhibit BAL features, we divide the sample into two subgroups based on M_{1450} : quasars brighter than $M_{1450} = -27$ and those fainter than $M_{1450} = -27$. We stack the [C II] spectra separately for each subgroup and find no significant (greater than 2σ) detection of a broad residual or a systematically blueshifted [C II] line in either stack. This result suggests that quasar brightness is unlikely to be the primary factor driving the broad [C II] outflows in BAL quasars, at least within our sample.

Due to the absence of spectral coverage for Mg II or rest-frame optical emission lines, we cannot reliably constrain black hole masses or Eddington ratios for our sample. However, previous studies have shown that the occurrence of BAL features is not strongly correlated with these properties⁶⁶, mitigating potential concerns about their influence on our findings.

A significant remaining caveat is the lack of precise constraints on the host galaxy masses, as differences in host properties could affect the interpretation of our results. We note that the mean Gaussian FWHMs of individual quasars are similar between the BAL ($4.3 \times 10^2 \text{ km s}^{-1}$) and non-BAL ($4.6 \times 10^2 \text{ km s}^{-1}$) samples, suggesting no strong difference in dynamical masses. Additionally, without Mg II coverage, we cannot determine whether any BAL quasars in our sample belong to the low-ionization BAL (LoBAL) subclass, which may be intrinsically distinct²⁴. Therefore, we cannot assess whether intrinsic physical differences between BAL and non-BAL host galaxies contribute to the observed differences in [C II] profiles.

Nevertheless, we conduct an additional robustness check to verify that the broad [C II] component detected in the BAL quasar stack is not simply due to statistical fluctuations arising from the small sample size or potential systematics from data reduction. We randomly select five quasars from the non-BAL group, stack their spectra, and measure the significance of any broad [C II] wing. Repeating this process 1,000 times, we find that the cumulative probability of randomly obtaining a broad wing with a significance equal to or greater than $S/N = 4.4$ is less than 2% (Figure A2). This test strongly suggests that the

broad [C II] component identified in the BAL quasar stack is unlikely to result from random noise or systematic errors in data reduction, continuum subtraction, or spectral stacking. Consequently, the link we observe between nuclear BAL outflows and large-scale [C II] outflows is likely to be genuine.

Robustness of Stacking Methods and Interpretation We note that ²² reported no clear evidence of [C II] outflows in quasar host galaxies at $z > 6$, although their high-resolution observations were not optimized for detecting outflows on kiloparsec scales (see also ^{21,23}). In their analysis, ²² employed UV-plane stacking (in addition to image-plane stacking) to enhance sensitivity and control for systematics arising from variable observing times and array configurations. In contrast, our dataset was collected using a uniform observational setup and consistent ALMA configurations, which already minimize these systematic concerns. Therefore, UV-plane stacking was unnecessary for our study. Nevertheless, as a consistency check, we performed image-plane stacking, as shown in Figure A3, confirming that our main conclusions remain unaffected by this stacking method. When directly stacking image cubes, the BAL sample still exhibits a broad [C II] component with a significance of 4.48σ , while the non-BAL stack remains below the 2σ detection threshold.

We caution that the method of continuum subtraction might still influence the visibility of the broad [C II] wing. However, we verified that using a zeroth-order polynomial continuum subtraction solely in the emission line spectral window in the uv domain does not change our results. Additionally, based on random stacking tests of non-BAL quasars (Figure A2), our continuum subtraction method is unlikely to introduce the observed blueshifted broad wing systematically. Throughout data reduction, we had no prior expectation of the broad [C II] component and consistently followed standard reduction procedures across the sample, further reducing potential systematic biases.

To examine the influence of individual quasars on our results, we conducted multiple tests:

1. The quasar J1513 exhibits a double-peaked [C II] profile, indicative of a rotating disk. Excluding this quasar does not affect our conclusions regarding the non-detection of a blueshifted broad component in the non-BAL stack.
2. Some ALMA spectra exhibit incomplete spectral coverage of the [C II] line (BAL: J0012; non-BAL: J1006 and J1016). Excluding these quasars, we find the broad component remains significant, with a reduced S/N of 2.85 for the BAL group (expected due to the smaller sample size; otherwise, still $S/N > 3$ with 5 quasars) and 1.78 for the non-BAL group. Although J0012's incomplete spectral coverage on the redshifted side may contribute to the detection of the broad wing, we argue that its intrinsic line profile — specifically, the presence of an extended wing — is the dominant factor in this contribution. As shown in Figure 1, J0012 exhibits a naturally broad [C II] profile, suggesting that the extended emission in the velocity space rather than spectral truncation is primarily responsible for its influence on the stacked spectrum.

3. To directly test the influence of individual sources, we performed jackknife tests by excluding one BAL quasar at a time and re-stacking the remaining four. The results are shown in Figure A4. In all five cases, the broad component remains significant, with measured significance values consistently greater than 2.8σ . The lowest value (2.85σ) occurs when J0012 is excluded, consistent with its individually broad profile but incomplete spectral coverage. These tests confirm that the observed broad [C II] wing in the BAL stack is not dominated by a single source.
4. To investigate the potential impact of host galaxy kinematics, we separated quasars into high- and low-FWHM groups (divided at 450 km s^{-1} , close to the mean or median FWHM). Neither group individually yields $> 3\sigma$ detection of a broad component (low-FWHM: 2.61σ , high-FWHM: 2.17σ), indicating that host galaxy kinematics alone do not explain the observed differences. The non-BAL group shows a broader range of line widths, yet does not show evidence for a broad wing, further arguing against FWHM-driven effects.
5. We tested normalization of spectra by their FWHM and amplitude, following procedures adopted by previous studies such as ²². This normalization is intended to account for variation in intrinsic [C II] line width across the sample, and mitigates biases due to particularly broad or narrow systems. The resulting velocity-normalized stacks are shown in Figure A5. While this normalization slightly reduces the broad-component significance in the BAL group to 2.8σ , the broad wing remains visible. The non-BAL group continues to show no significant broad component (1.0σ). This suggests that the detected outflow feature in BAL quasars is not an artifact of stacking systems with broader intrinsic lines. However, we caution that this normalization might dilute weak broad wings, especially if the wing and the line core have different physical origins. Thus, the lower significance in this test may reflect an underestimation of true broad wing strength.
6. For ESI spectra, due to limited wavelength coverage and uncertainties from telluric absorption, weak BAL features might be ambiguous. To address this, we separately stacked only the most robust BAL quasars ($BI_0 > 2500 \text{ km s}^{-1}$; J2317, J2325) against definitive non-BAL quasars ($BI_0 = 0$; J0120, J0231, J0306, J1500, J1513, J1614), normalizing by both amplitude and FWHM. We still detect a broad component at 2.38σ for the robust BAL subgroup versus 1.15σ for definitive non-BAL quasars, reinforcing the robustness of our conclusion despite smaller samples.

Collectively, these tests demonstrate that the observed [C II] broad component in the BAL quasar stack is robust to continuum subtraction, sample size, normalization method, and individual object exclusion. We emphasize that our BAL sample, while modest, already represents the largest high-redshift BAL quasar sample with uniform [C II] observations currently available, built up over the past five years. Future studies incorporating $z > 6$ BAL quasars may help further increase sample size

and improve constraints on the connection between nuclear and galactic-scale outflows during the reionization epoch.

Data Availability

The ALMA data used in this study are publicly available from the ALMA Science Archive at <https://almascience.nrao.edu>, under the project code: ADS/JAO.ALMA#2022.1.00662.S. The reduced Keck/ESI spectra used for BAL classification are available at <https://github.com/yzhuastro/data-zhu25-qso>. The raw ESI data can be accessed via the Keck Observatory Archive (KOA) at <https://koa.ipac.caltech.edu>.

Code Availability

The ALMA data were reduced using the publicly available software CARTA⁶⁷. The Keck/ESI spectra were reduced using a custom pipeline written in GDL⁴⁵. Analysis was performed using Astropy⁶⁸, NumPy⁶⁹, and Matplotlib⁷⁰. The illustration in Figure 3 was created with Adobe Fresco (<https://www.adobe.com/products/fresco.html>).

Acknowledgments

YZ, MJR, YS, GHR, and ZJ acknowledge support from the NIRCам Science Team contract to the University of Arizona, NAS5-02015. This work was supported by the NSF through award SOSPADA-029 from the NRAO. YZ and GDB were supported by the NSF through grant AST-1751404. LCH was supported by the National Science Foundation of China (12233001) and the National Key R&D Program of China (2022YFF0503401). FY is supported by the Natural Science Foundation of China (grants 12133008, 12192220, 12192223, and 12361161601), the China Manned Space Program through its Space Application System, and the National Key R&D Program of China No. 2023YFB3002502. TTT has been supported by the Japan Society for the Promotion of Science (JSPS) Grants-in-Aid for Scientific Research (24H00247). This work has also been supported in part by the Collaboration Funding of the Institute of Statistical Mathematics “Machine-Learning-Based Cosmogony: From Structure Formation to Galaxy Evolution”. This manuscript benefited from grammar checking and proofreading using ChatGPT (OpenAI; <https://openai.com/chatgpt>). This paper makes use of the following ALMA data: ADS/JAO.ALMA#2022.1.00662.S. ALMA is a partnership of ESO (representing its member states), NSF (USA) and NINS (Japan), together with NRC (Canada), MOST and ASIAA (Taiwan), and KASI (Republic of Korea), in cooperation with the Republic of Chile. The Joint ALMA Observatory is operated by ESO, AUI/NRAO and NAOJ. The National Radio Astronomy Observatory and Green Bank Observatory are facilities of the U.S. National Science Foundation operated under cooperative agreement by Associated Universities, Inc. Some of the data presented herein were obtained at Keck Observatory, which is a private 501(c)3 non-profit organization operated as a scientific partnership among the California Institute of Technology, the University of California, and the National Aeronautics and Space Administration. The Observatory was made possible by the generous financial support of the W. M.

Keck Foundation. The authors wish to recognize and acknowledge the very significant cultural role and reverence that the summit of Maunakea has always had within the Native Hawaiian community. We are most fortunate to have the opportunity to conduct observations from this mountain. This research has made use of the Keck Observatory Archive (KOA), which is operated by the W. M. Keck Observatory and the NASA Exoplanet Science Institute (NExScI), under contract with the National Aeronautics and Space Administration.

Author Contributions

YZ led the observations and data reduction for the ALMA and ESI programs, performed the initial analysis, and wrote the first draft. MJR, LCH, YS, GHR, and FY contributed to the initial discussions and interpretation of the results. TJLCB, GDB, and JY assisted with observations and sample selection. EB and MB contributed to the analysis methodology and statistical interpretation. The remaining authors provided helpful comments and discussions.

Competing interests

The authors declare no competing interests.

1. Kormendy, J. & Ho, L. C. Coevolution (Or Not) of Supermassive Black Holes and Host Galaxies. *Annual Review of Astronomy and Astrophysics* **51**, 511–653 (2013). URL <https://ui.adsabs.harvard.edu/abs/2013ARA&A..51..511K>. ADS Bibcode: 2013ARA&A..51..511K.
2. Sun, Y. *et al.* No Evidence for a Significant Evolution of M_{\bullet} – M_{\star} Relation in Massive Galaxies up to $z \sim 4$. *The Astrophysical Journal* **978**, 98 (2025). URL <https://ui.adsabs.harvard.edu/abs/2025ApJ...978...98S>. Publisher: IOP ADS Bibcode: 2025ApJ...978...98S.
3. Inayoshi, K., Visbal, E. & Haiman, Z. The Assembly of the First Massive Black Holes. *Annual Review of Astronomy and Astrophysics* **58**, 27–97 (2020). URL <https://ui.adsabs.harvard.edu/abs/2020ARA&A..58...27I>. ArXiv: 1911.05791.
4. Weymann, R. J., Morris, S. L., Foltz, C. B. & Hewett, P. C. Comparisons of the Emission-Line and Continuum Properties of Broad Absorption Line and Normal Quasi-stellar Objects. *The Astrophysical Journal* **373**, 23 (1991). URL <https://ui.adsabs.harvard.edu/abs/1991ApJ...373...23W>. Publisher: IOP ADS Bibcode: 1991ApJ...373...23W.
5. Maiolino, R. *et al.* Evidence of strong quasar feedback in the early Universe. *Monthly Notices of the Royal Astronomical Society* **425**, L66–L70 (2012). URL <https://ui.adsabs.harvard.edu/abs/2012MNRAS.425L..66M>. Publisher: OUP ADS Bibcode: 2012MNRAS.425L..66M.
6. Veilleux, S., Maiolino, R., Bolatto, A. D. & Aalto, S. Cool outflows in galaxies and their implications. *Astronomy and Astrophysics Review* **28**, 2 (2020). URL <https://ui.adsabs.harvard.edu/abs/2020A&ARv...28....2V>. Publisher: Springer ADS Bibcode: 2020A&ARv...28....2V.
7. Juodžbalis, I. *et al.* A dormant overmassive black hole in the early Universe. *Nature* **636**, 594–597 (2024). URL <https://ui.adsabs.harvard.edu/abs/2024Natur.636..594J>. ADS Bibcode: 2024Natur.636..594J.
8. Sun, Y. *et al.* The M_{\bullet} – M_{\star} Relation Evolution from $z \sim 6$ to the Present Epoch (2025). URL <https://ui.adsabs.harvard.edu/abs/2025arXiv250303675S>. Publication Title: arXiv e-prints ADS Bibcode: 2025arXiv250303675S.

9. Stacey, G. J. *et al.* The 158 Micron [C ii] Line: A Measure of Global Star Formation Activity in Galaxies. *The Astrophysical Journal* **373**, 423 (1991). URL <https://ui.adsabs.harvard.edu/abs/1991ApJ...373..423S>. Publisher: IOP ADS Bibcode: 1991ApJ...373..423S.
10. Carilli, C. L. & Walter, F. Cool Gas in High-Redshift Galaxies. *Annual Review of Astronomy and Astrophysics* **51**, 105–161 (2013). URL <https://ui.adsabs.harvard.edu/abs/2013ARA&A..51..105C>. ADS Bibcode: 2013ARA&A..51..105C.
11. Lagache, G., Cousin, M. & Chatzikos, M. The [CII] 158 μm line emission in high-redshift galaxies. *Astronomy and Astrophysics* **609**, A130 (2018). URL <https://ui.adsabs.harvard.edu/abs/2018A&A...609A.130L>. ADS Bibcode: 2018A&A...609A.130L.
12. Gullberg, B. *et al.* The nature of the [C II] emission in dusty star-forming galaxies from the SPT survey. *Monthly Notices of the Royal Astronomical Society* **449**, 2883–2900 (2015). URL <https://ui.adsabs.harvard.edu/abs/2015MNRAS.449.2883G>. Publisher: OUP ADS Bibcode: 2015MNRAS.449.2883G.
13. Jones, G. C. *et al.* Dynamical Characterization of Galaxies at $z \sim 4$ –6 via Tilted Ring Fitting to ALMA [C II] Observations. *The Astrophysical Journal* **850**, 180 (2017). URL <https://ui.adsabs.harvard.edu/abs/2017ApJ...850..180J>. Publisher: IOP ADS Bibcode: 2017ApJ...850..180J.
14. Ciccone, C. *et al.* Very extended cold gas, star formation and outflows in the halo of a bright quasar at $z > 6$. *Astronomy and Astrophysics* **574**, A14 (2015). URL <https://ui.adsabs.harvard.edu/abs/2015A&A...574A..14C>. ADS Bibcode: 2015A&A...574A..14C.
15. Meyer, R. A. *et al.* Physical Constraints on the Extended Interstellar Medium of the $z = 6.42$ Quasar J1148+5251: [C II]158 μm , [N II]205 μm , and [O I]146 μm Observations. *The Astrophysical Journal* **927**, 152 (2022). URL <https://ui.adsabs.harvard.edu/abs/2022ApJ...927..152M>. Publisher: IOP ADS Bibcode: 2022ApJ...927..152M.
16. Ginolfi, M. *et al.* Molecular gas on large circumgalactic scales at $z = 3.47$. *Monthly Notices of the Royal Astronomical Society* **468**, 3468–3483 (2017). URL <https://ui.adsabs.harvard.edu/abs/2017MNRAS.468.3468G>. Publisher: OUP ADS Bibcode: 2017MNRAS.468.3468G.
17. Ginolfi, M. *et al.* The ALPINE-ALMA [C II] survey: Star-formation-driven outflows and circumgalactic enrichment in the early Universe. *Astronomy and Astrophysics* **633**, A90 (2020). URL <https://ui.adsabs.harvard.edu/abs/2020A&A...633A..90G>. Publisher: EDP ADS Bibcode: 2020A&A...633A..90G.
18. Herrera-Camus, R. *et al.* Kiloparsec view of a typical star-forming galaxy when the Universe was ~ 1 Gyr old. I. Properties of outflow, halo, and interstellar medium. *Astronomy and Astrophysics* **649**, A31 (2021). URL <https://ui.adsabs.harvard.edu/abs/2021A&A...649A..31H>. Publisher: EDP ADS Bibcode: 2021A&A...649A..31H.
19. Spilker, J. S. *et al.* Ubiquitous Molecular Outflows in $z > 4$ Massive, Dusty Galaxies. I. Sample Overview and Clumpy Structure in Molecular Outflows on 500 pc Scales. *The Astrophysical Journal* **905**, 85 (2020). URL <https://ui.adsabs.harvard.edu/abs/2020ApJ...905...85S>. Publisher: IOP ADS Bibcode: 2020ApJ...905...85S.
20. Birkin, J. E. *et al.* The ALMA-CRISTAL Survey: Weak Evidence for Star-formation-driven Outflows in $z \sim 5$ Main-sequence Galaxies. *The Astrophysical Journal* **985**, 243 (2025). URL <https://ui.adsabs.harvard.edu/abs/2025ApJ...985..243B>. Publisher: IOP ADS Bibcode: 2025ApJ...985..243B.
21. Decarli, R. *et al.* An ALMA [C II] Survey of 27 Quasars at $z > 5.94$. *The Astrophysical Journal* **854**, 97 (2018). URL <https://ui.adsabs.harvard.edu/abs/2018ApJ...854...97D>.
22. Novak, M. *et al.* No Evidence for [C II] Halos or High-velocity Outflows in $z \gtrsim 6$ Quasar Host Galaxies. *The Astrophysical Journal* **904**, 131 (2020). URL <https://ui.adsabs.harvard.edu/abs/2020ApJ...904..131N>. Publisher: IOP ADS Bibcode: 2020ApJ...904..131N.
23. Sawamura, M. *et al.* No Galaxy-scale [C II] Fast Outflow in the $z = 6.72$ Red Quasar HSC J1205–0000. *The Astrophysical Journal* **980**, 121 (2025). URL <https://ui.adsabs.harvard.edu/abs/2025ApJ...980..121S>. Publisher: IOP ADS Bibcode: 2025ApJ...980..121S.
24. Bischetti, M. *et al.* Multiphase Black Hole Feedback and a Bright [C II] Halo in a LoBAL Quasar at $z \sim 6.6$. *The Astrophysical Journal* **970**, 9 (2024). URL <https://ui.adsabs.harvard.edu/abs/2024ApJ...970....9B>. Publisher: IOP ADS Bibcode: 2024ApJ...970....9B.
25. Carniani, S., Maiolino, R., Smit, R. & Amorín, R. ALMA Detection of Extended [C II] Emission in Himiko at $z = 6.6$. *The Astrophysical Journal* **854**, L7 (2018). URL <https://ui.adsabs.harvard.edu/abs/2018ApJ...854L...7C>. Publisher: IOP ADS Bibcode: 2018ApJ...854L...7C.
26. Izumi, T. *et al.* Subaru High- z Exploration of Low-luminosity Quasars (SHELLQs). XII. Extended [C II] Structure (Merger or Outflow) in a $z = 6.72$ Red Quasar. *The Astrophysical Journal* **908**, 235 (2021). URL <https://ui.adsabs.harvard.edu/abs/2021ApJ...908..235I>. Publisher: IOP ADS Bibcode: 2021ApJ...908..235I.
27. Murray, N., Chiang, J., Grossman, S. A. & Voit, G. M. Accretion Disk Winds from Active Galactic Nuclei. *The Astrophysical Journal* **451**, 498 (1995). URL <https://ui.adsabs.harvard.edu/abs/1995ApJ...451..498M>. Publisher: IOP ADS Bibcode: 1995ApJ...451..498M.
28. Proga, D., Stone, J. M. & Kallman, T. R. Dynamics of Line-driven Disk Winds in Active Galactic Nuclei. *The Astrophysical Journal* **543**, 686–696 (2000). URL <https://ui.adsabs.harvard.edu/abs/2000ApJ...543..686P>. Publisher: IOP ADS Bibcode: 2000ApJ...543..686P.
29. Elvis, M. A Structure for Quasars. *The Astrophysical Journal* **545**, 63–76 (2000). URL <https://ui.adsabs.harvard.edu/abs/2000ApJ...545...63E>. Publisher: IOP ADS Bibcode: 2000ApJ...545...63E.
30. Bischetti, M. *et al.* Suppression of black-hole growth by strong outflows at redshifts 5.8–6.6. *Nature* **605**, 244–247 (2022). URL <https://ui.adsabs.harvard.edu/abs/2022Natur.605..244B>. ADS Bibcode: 2022Natur.605..244B.
31. D’Odorico, V. *et al.* XQR-30: The ultimate XSHOOTER quasar sample at the reionization epoch. *Monthly Notices of the Royal Astronomical Society* **523**, 1399–1420 (2023). URL <https://ui.adsabs.harvard.edu/abs/2023MNRAS.523.1399D>. Publisher: OUP ADS Bibcode: 2023MNRAS.523.1399D.
32. Bosman, S. E. I. *et al.* Hydrogen reionization ends by $z = 5.3$: Lyman- α optical depth measured by the XQR-30 sample. *Monthly Notices of the Royal Astronomical Society* **514**, 55–76 (2022). URL <https://ui.adsabs.harvard.edu/abs/2022MNRAS.514...55B>. ADS Bibcode: 2022MNRAS.514...55B.
33. Zhu, Y. *et al.* Long Dark Gaps in the Ly β Forest at $z < 6$: Evidence of Ultra-late Reionization from XQR-30 Spectra. *The Astrophysical Journal* **932**, 76 (2022). URL <https://ui.adsabs.harvard.edu/abs/2022ApJ...932...76Z>. ADS Bibcode: 2022ApJ...932...76Z.
34. Planck Collaboration *et al.* Planck 2018 results. VI. Cosmological parameters. *Astronomy and Astrophysics* **641**, A6 (2020). URL <http://ui.adsabs.harvard.edu/abs/2020A&A...641A...6P>.
35. Astropy Collaboration *et al.* The Astropy Project: Building an Open-science Project and Status of the v2.0 Core Package. *The Astronomical Journal* **156**, 123 (2018). URL <https://ui.adsabs.harvard.edu/abs/2018AJ...156..123A>.
36. Yang, J. *et al.* Discovery of 16 New $z \sim 5.5$ Quasars: Filling in the Redshift Gap of Quasar Color Selection. *The Astronomical Journal* **153**, 184 (2017). URL <https://ui.adsabs.harvard.edu/abs/2017AJ...153..184Y>.

- harvard.edu/abs/2017AJ....153..184Y. ADS Bibcode: 2017AJ....153..184Y.
37. Yang, J. *et al.* Filling in the Quasar Redshift Gap at $z \sim 5.5$. II. A Complete Survey of Luminous Quasars in the Post-reionization Universe. *The Astrophysical Journal* **871**, 199 (2019). URL <https://ui.adsabs.harvard.edu/abs/2019ApJ...871..199Y>. ADS Bibcode: 2019ApJ...871..199Y.
 38. Zhu, Y. *et al.* Probing Ultralate Reionization: Direct Measurements of the Mean Free Path over $5 < z < 6$. *The Astrophysical Journal* **955**, 115 (2023). URL <https://ui.adsabs.harvard.edu/abs/2023ApJ...955..115Z>. ADS Bibcode: 2023ApJ...955..115Z.
 39. McMullin, J. P., Waters, B., Schiebel, D., Young, W. & Golap, K. CASA Architecture and Applications **376**, 127 (2007). URL <https://ui.adsabs.harvard.edu/abs/2007ASPC..376..127M>. Conference Name: Astronomical Data Analysis Software and Systems XVI ADS Bibcode: 2007ASPC..376..127M.
 40. CASA Team *et al.* CASA, the Common Astronomy Software Applications for Radio Astronomy. *Publications of the Astronomical Society of the Pacific* **134**, 114501 (2022). URL <https://ui.adsabs.harvard.edu/abs/2022PASP..134k4501C>. ADS Bibcode: 2022PASP..134k4501C.
 41. Eilers, A.-C. *et al.* Detecting and Characterizing Young Quasars. I. Systemic Redshifts and Proximity Zone Measurements. *The Astrophysical Journal* **900**, 37 (2020). URL <http://adsabs.harvard.edu/abs/2020ApJ...900...37E>.
 42. Zhu, Y. *et al.* Discovery of a Unique Close Quasar–DSFG Pair Linked by a [C II] Bridge at $z = 5.63$. *Research Notes of the American Astronomical Society* **8**, 284 (2024). URL <https://ui.adsabs.harvard.edu/abs/2024RNAAS...8..284Z>. Publisher: IOP ADS Bibcode: 2024RNAAS...8..284Z.
 43. Dopita, M. *et al.* The Wide Field Spectrograph (WiFeS). *Astrophysics and Space Science* **310**, 255–268 (2007). URL <https://ui.adsabs.harvard.edu/abs/2007Ap&SS.310..255D>. Publisher: Springer ADS Bibcode: 2007Ap&SS.310..255D.
 44. Dopita, M. *et al.* The Wide Field Spectrograph (WiFeS): performance and data reduction. *Astrophysics and Space Science* **327**, 245–257 (2010). URL <https://ui.adsabs.harvard.edu/abs/2010Ap&SS.327..245D>. Publisher: Springer ADS Bibcode: 2010Ap&SS.327..245D.
 45. Coulais, A. *et al.* Status of GDL - GNU Data Language **434**, 187 (2010). URL <https://ui.adsabs.harvard.edu/abs/2010ASPC..434..187C>. Conference Name: Astronomical Data Analysis Software and Systems XIX Place: eprint: arXiv:1101.0679 ADS Bibcode: 2010ASPC..434..187C.
 46. Becker, G. D. *et al.* The Evolution of O I over $3.2 < z < 6.5$: Reionization of the Circumgalactic Medium. *The Astrophysical Journal* **883**, 163 (2019). URL <http://adsabs.harvard.edu/abs/2019ApJ...883..163B>.
 47. Kelson, D. D. Optimal Techniques in Two-dimensional Spectroscopy: Background Subtraction for the 21st Century. *Publications of the Astronomical Society of the Pacific* **115**, 688–699 (2003). URL <http://adsabs.harvard.edu/abs/2003PASP..115..688K>.
 48. Horne, K. An optimal extraction algorithm for CCD spectroscopy. *Publications of the Astronomical Society of the Pacific* **98**, 609–617 (1986). URL <http://adsabs.harvard.edu/abs/1986PASP...98..609H>.
 49. Noll, S. *et al.* An atmospheric radiation model for Cerro Paranal. I. The optical spectral range. *Astronomy and Astrophysics* **543**, A92 (2012). URL <http://adsabs.harvard.edu/abs/2012A&26A...543A..92N>.
 50. Jones, A., Noll, S., Kausch, W., Szyszka, C. & Kimeswenger, S. An advanced scattered moonlight model for Cerro Paranal. *Astronomy and Astrophysics* **560**, A91 (2013). URL <http://adsabs.harvard.edu/abs/2013A&26A...560A..91J>.
 51. Gibson, R. R. *et al.* A Catalog of Broad Absorption Line Quasars in Sloan Digital Sky Survey Data Release 5. *The Astrophysical Journal* **692**, 758–777 (2009). URL <https://ui.adsabs.harvard.edu/abs/2009ApJ...692..758G>. Publisher: IOP ADS Bibcode: 2009ApJ...692..758G.
 52. Tanner, R. & Weaver, K. A. Simulations of AGN-driven Galactic Outflow Morphology and Content. *The Astronomical Journal* **163**, 134 (2022). URL <https://ui.adsabs.harvard.edu/abs/2022AJ....163..134T>. Publisher: IOP ADS Bibcode: 2022AJ....163..134T.
 53. Stanley, F., Jolly, J. B., König, S. & Knudsen, K. K. A spectral stacking analysis to search for faint outflow signatures in $z \sim 6$ quasars. *Astronomy and Astrophysics* **631**, A78 (2019). URL <https://ui.adsabs.harvard.edu/abs/2019A&A...631A..78S>. Publisher: EDP ADS Bibcode: 2019A&A...631A..78S.
 54. Xu, X., Arav, N., Miller, T. & Benn, C. VLT/X-Shooter Survey of BAL Quasars: Large Distance Scale and AGN Feedback. *The Astrophysical Journal* **876**, 105 (2019). URL <https://ui.adsabs.harvard.edu/abs/2019ApJ...876..105X>. Publisher: IOP ADS Bibcode: 2019ApJ...876..105X.
 55. Liu, W. *et al.* Galactic Winds across the Gas-rich Merger Sequence. II. Ly α Emission and Highly Ionized O VI and N V Outflows in Ultraluminous Infrared Galaxies. *The Astrophysical Journal* **934**, 160 (2022). URL <https://ui.adsabs.harvard.edu/abs/2022ApJ...934..160L>. Publisher: IOP ADS Bibcode: 2022ApJ...934..160L.
 56. Veilleux, S. *et al.* Galactic Winds across the Gas-rich Merger Sequence. I. Highly Ionized N V and O VI Outflows in the QUEST Quasars. *The Astrophysical Journal* **926**, 60 (2022). URL <https://ui.adsabs.harvard.edu/abs/2022ApJ...926...60V>. Publisher: IOP ADS Bibcode: 2022ApJ...926...60V.
 57. Hewett, P. C. & Foltz, C. B. The Frequency and Radio Properties of Broad Absorption Line Quasars. *The Astronomical Journal* **125**, 1784–1794 (2003). URL <https://ui.adsabs.harvard.edu/abs/2003AJ....125.1784H>. Publisher: IOP ADS Bibcode: 2003AJ....125.1784H.
 58. Bischetti, M. *et al.* Widespread QSO-driven outflows in the early Universe. *Astronomy and Astrophysics* **630**, A59 (2019). URL <https://ui.adsabs.harvard.edu/abs/2019A&A...630A..59B>. ADS Bibcode: 2019A&A...630A..59B.
 59. Hailey-Dunsheath, S. *et al.* Detection of the 158 μm [C II] Transition at $z = 1.3$: Evidence for a Galaxy-wide Starburst. *The Astrophysical Journal* **714**, L162–L166 (2010). URL <https://ui.adsabs.harvard.edu/abs/2010ApJ...714L.162H>. Publisher: IOP ADS Bibcode: 2010ApJ...714L.162H.
 60. Fiore, F. *et al.* AGN wind scaling relations and the co-evolution of black holes and galaxies. *Astronomy and Astrophysics* **601**, A143 (2017). URL <https://ui.adsabs.harvard.edu/abs/2017A&A...601A.143F>. ADS Bibcode: 2017A&A...601A.143F.
 61. McMillan, P. J. The mass distribution and gravitational potential of the Milky Way. *Monthly Notices of the Royal Astronomical Society* **465**, 76–94 (2017). URL <http://adsabs.harvard.edu/abs/2017MNRAS.465...76M>.
 62. Zhu, Y. *et al.* How close dark matter haloes and MOND are to each other: three-dimensional tests based on Gaia DR2. *Monthly Notices of the Royal Astronomical Society* **519**, 4479–4498 (2023). URL <https://ui.adsabs.harvard.edu/abs/2023MNRAS.519.4479Z>. ADS Bibcode: 2023MNRAS.519.4479Z.
 63. Molina, J. *et al.* Enhanced Star Formation Efficiency in the Central Regions of Nearby Quasar Hosts. *The Astrophysical Journal* **944**, 30 (2023). URL <https://ui.adsabs.harvard.edu/abs/2023ApJ...944...30M>. Publisher: IOP ADS Bibcode: 2023ApJ...944...30M.
 64. Bañados, E. *et al.* The $z = 7.54$ Quasar ULAS J1342+0928 Is Hosted by a Galaxy Merger. *The Astrophysical Journal* **881**, L23 (2019). URL <https://ui.adsabs.harvard.edu/abs/2019ApJ...881L..23B>. Publisher: IOP ADS Bibcode: 2019ApJ...881L..23B.

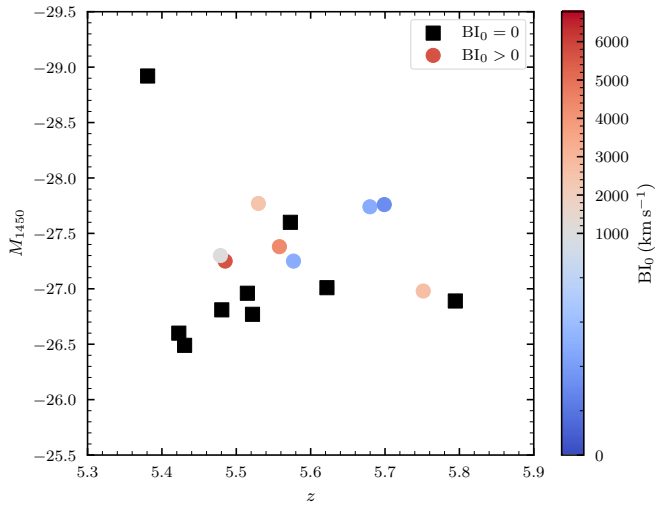


Figure A1 – UV magnitude (M_{1450}) versus redshift for the quasars used in this work. The five quasars with strong BAL features ($BI_0 > 1000 \text{ km s}^{-1}$) are used to create the stacked [C II] profile shown in Figure 3(a).

65. Izumi, T. *et al.* Subaru High- z Exploration of Low-luminosity Quasars (SHELLQs). XIII. Large-scale Feedback and Star Formation in a Low-luminosity Quasar at $z = 7.07$ on the Local Black Hole to Host Mass Relation. *The Astrophysical Journal* **914**, 36 (2021). URL <https://ui.adsabs.harvard.edu/abs/2021ApJ...914...36I>. Publisher: IOP ADS Bibcode: 2021ApJ...914...36I.
66. Bischetti, M. *et al.* The fraction and kinematics of broad absorption line quasars across cosmic time (2023). URL <https://ui.adsabs.harvard.edu/abs/2023arXiv230109731B>. Publication Title: arXiv e-prints ADS Bibcode: 2023arXiv230109731B.
67. Comrie, A. *et al.* CARTA: The Cube Analysis and Rendering Tool for Astronomy. *Zenodo* (2021). URL <https://ui.adsabs.harvard.edu/abs/2021zndo...3377984C>. Publisher: Zenodo ADS Bibcode: 2021zndo...3377984C.
68. Astropy Collaboration *et al.* The Astropy Project: Sustaining and Growing a Community-oriented Open-source Project and the Latest Major Release (v5.0) of the Core Package. *The Astrophysical Journal* **935**, 167 (2022). URL <https://ui.adsabs.harvard.edu/abs/2022ApJ...935..167A>. Publisher: IOP ADS Bibcode: 2022ApJ...935..167A.
69. van der Walt, S., Colbert, S. C. & Varoquaux, G. The NumPy Array: A Structure for Efficient Numerical Computation. *Computing in Science and Engineering* **13**, 22–30 (2011). URL <http://adsabs.harvard.edu/abs/2011CSE....13b..22V>.
70. Hunter, J. D. Matplotlib: A 2D Graphics Environment. *Computing in Science and Engineering* **9**, 90–95 (2007). URL <http://adsabs.harvard.edu/abs/2007CSE.....9...90H>.

A Supplementary Figures

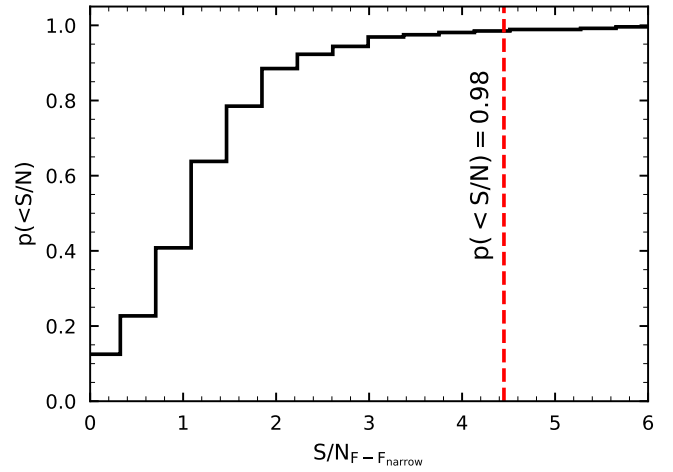


Figure A2 – Cumulative distribution of the S/N of the broad component based on random stacks of five non-BAL quasars. The probability of reproducing an $S/N=4.4$ detection of the broad [C II] component in non-BAL quasars is less than 0.02. This test indicates that the observed broad component in the BAL quasar stack is unlikely to result from statistical fluctuations due to small sample size. Additionally, it suggests that systematic effects in data reduction or continuum subtraction are not responsible for the detection.

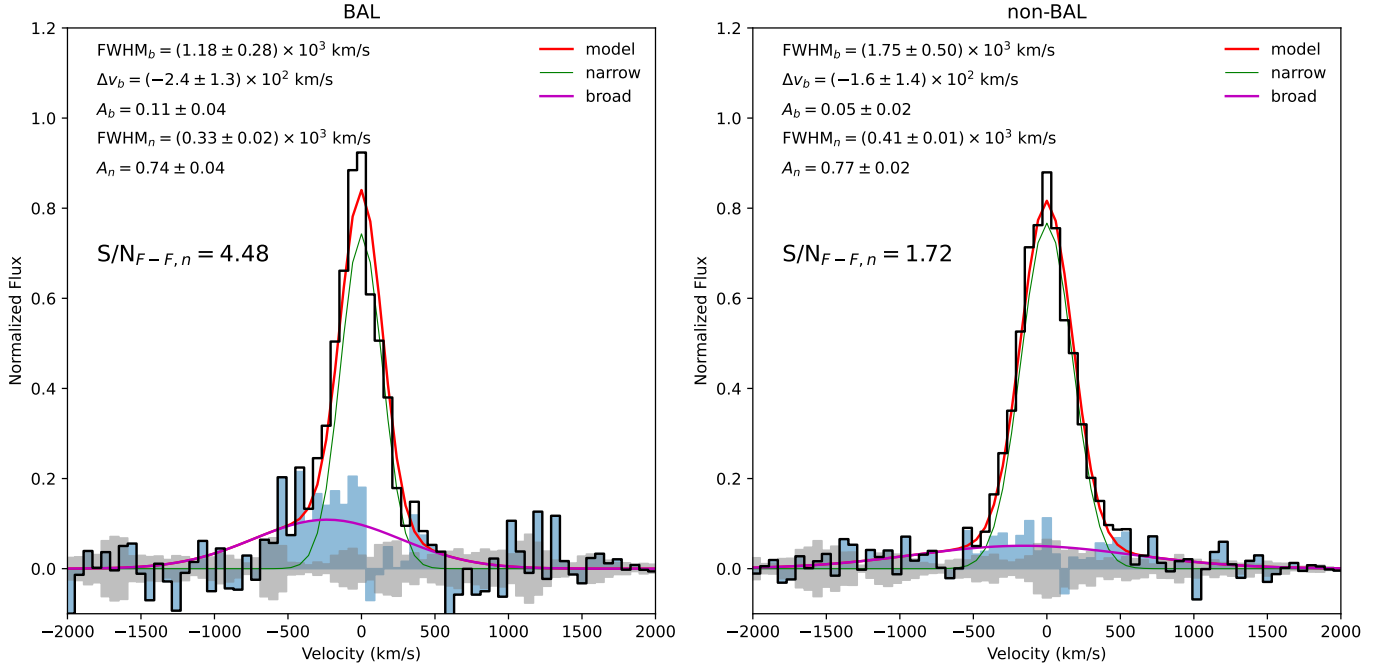
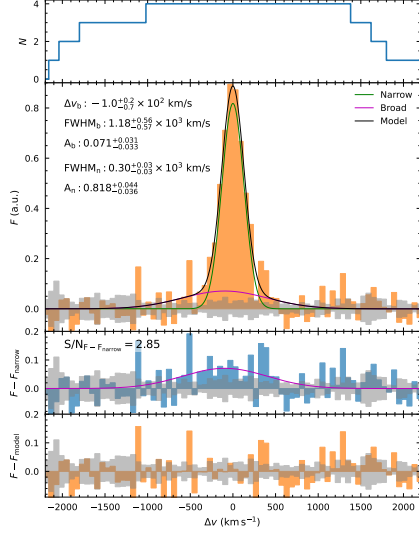
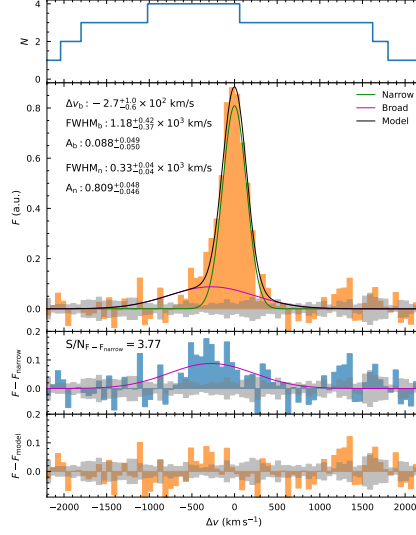


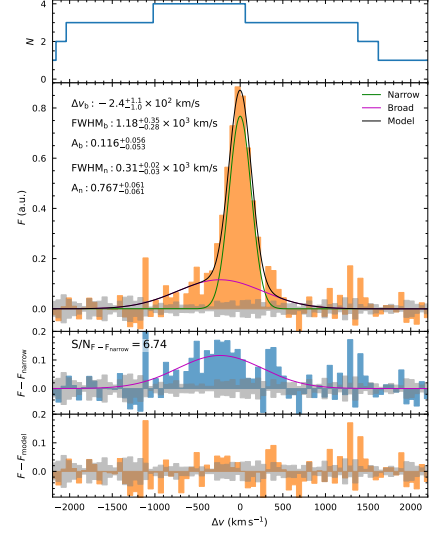
Figure A3 – [C II] emission from the stacked image cubes of BAL (left panel) and non-BAL (right panel) quasars. The black curves represent the normalized flux (arbitrary units), while the blue shaded regions show the residual flux after subtracting the narrow component. The gray shaded regions indicate the $\pm 1\sigma$ noise level. The fitting parameter uncertainties shown in this plot are derived from a single stack, rather than the bootstrap approach used in Figure 3. When stacking image cubes instead of 1D spectra, the BAL sample still exhibits a significant broad component at 4.48σ , whereas the non-BAL sample remains below the 2σ detection threshold.



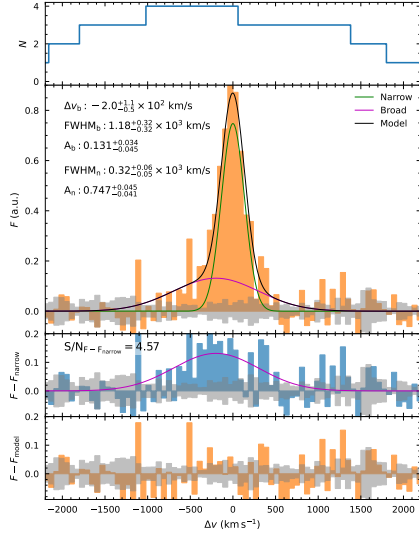
(a) Excluding J0012



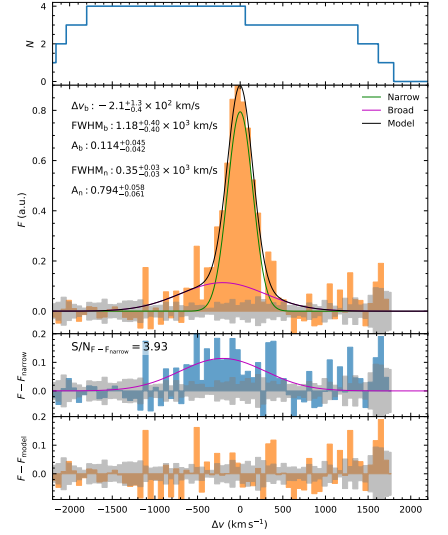
(b) Excluding J1022



(c) Excluding J2207

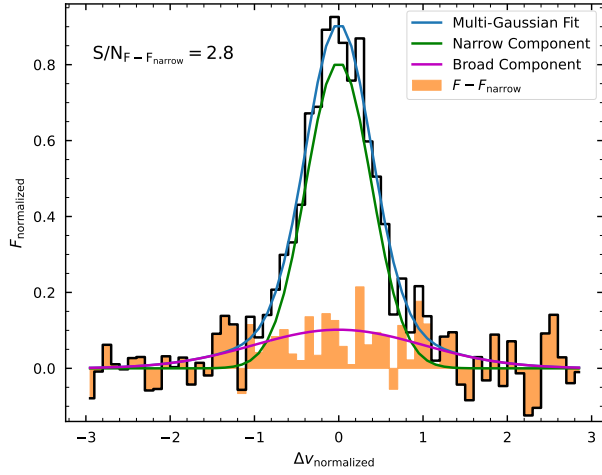


(d) Excluding J2317

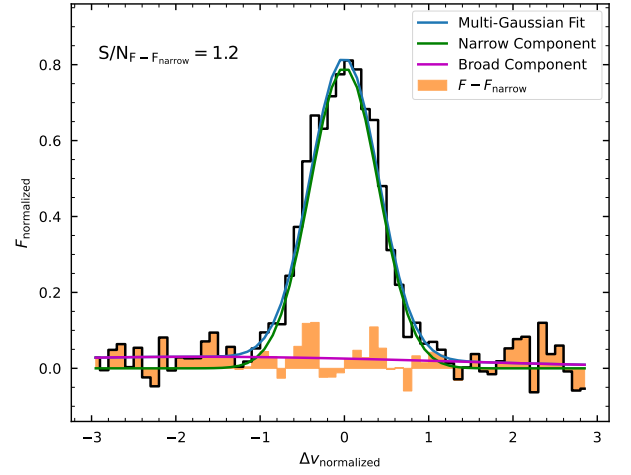


(e) Excluding J2325

Figure A4 – Jackknife tests of the [C II] stacked spectrum for the BAL QSO sample. Each panel shows the stack of 4 out of 5 BAL quasars, with one excluded. The broad component remains visible across all tests, indicating that the result is not driven by any single source, although might be boosted by J0012.



(a) BAL stack (velocity-normalized)



(b) non-BAL stack (velocity-normalized)

Figure A5 – Velocity-normalized stacking of [C II] spectra for the BAL (panel a) and non-BAL (panel b) quasar samples. Each individual profile has been normalized by its FWHM before stacking. A broad component remains visible in the BAL stack, while the non-BAL stack shows no significant excess. This confirms that the detected wing is not an artifact from different velocity widths.